16èmes Journées de l'Hydrodynamique

27-29 novembre 2018 - Marseille

Modélisation du déferlement dû à la bathymétrie dans un code de simulation des vagues non-linéaires et dispersives en zone côtière

Modeling of depth-induced wave breaking in a simulation code for nonlinear and dispersive waves in the coastal zone

B. SIMON[(1)], C. PAPOUTSELLIS[(1,2)], M. BENOIT[(1,3)], M. YATES[(2,4)]

simon@irphe.univ-mrs.fr ; cpapoutsellis@gmail.com ; benoit@irphe.univ-mrs.fr ; marissa.yates@cerema.fr

[(1)] Aix Marseille Univ, CNRS, Centrale Marseille, Irphé (UMR 7342), Marseille
[(2)] Laboratoire d'Hydraulique Saint-Venant, Ecole des Ponts, Cerema, EDF, Université Paris-Est, Chatou
[(3)] Ecole Centrale de Marseille, Marseille
[(4)] Cerema, Water, Sea and Rivers, Environment and Risks Department, Plouzané

Résumé

La modélisation de la dissipation d'énergie due au déferlement en eau peu profonde dans un code de vagues complètement non-linéaire et dispersif est étudiée. Le modèle de propagation des vagues est fondé sur la théorie potentielle et suppose au départ que la surface libre ne se retourne pas. L'inclusion de la dissipation par déferlement est toutefois possible en ajoutant un terme similaire à une pression dans la condition limite dynamique de surface libre. Deux critères issus de la littérature sont testés pour déterminer le début de déferlement, l'un de type géométrique et l'autre de type énergétique. Deux méthodes sont testées afin de dissiper l'énergie, l'une basée sur la similarité d'une vague déferlante avec un ressaut hydraulique déferlant et l'autre utilisant un terme dissipatif de type viscosité turbulente. Les simulations numériques sont effectuées à l'aide de combinaisons des deux critères et des deux méthodes de dissipation. Leurs résultats sont comparés à des expériences des vagues déferlant sur une barre immergée, d'abord pour des vagues régulières, puis pour des vagues irrégulières. Nous montrons que les différentes approches sont capables de reproduire les évolutions des trains de vagues observées expérimentalement, bien que des tests supplémentaires restent à mener pour valider complètement le modèle dans une gamme de conditions plus large.

Summary

The modeling of wave breaking dissipation in shallow water within a fully nonlinear and dispersive wave model is investigated. The wave propagation model is based on potential flow theory and initially assumes non-overturning waves. Inclusion of breaking dissipation is however possible by adding a pressure-like term to the dynamic free surface boundary condition. Two criteria from the literature are tested to determine the onset of breaking, one geometric and another energetic. Two methods are tested in order to dissipate the energy due to breaking, the first based on the analogy of a breaking wave with a breaking hydraulic jump, and the second relying on an eddy viscosity dissipative term. Numerical simulations are performed using combinations of the two criteria and the two dissipation methods. The results are compared with experiments of waves breaking over a submerged bar, considering first regular waves, and then irregular waves. It is shown that the different approaches are able to reproduce the wave transformation observed in the experiments, although additional tests remain to be performed to fully validate the model for a wider range of conditions.

I – Introduction

As ocean waves propagate towards the shore, they evolve under the effects of several physical processes, among which shoaling, refraction and breaking play a dominant role. Accurate modeling of these processes requires a mathematical approach that properly simulates both dispersive and nonlinear effects. One option is to use CFD codes to model in detail all of the physical processes, but this approach is computationally costly and can be applied at local scales only.

Another faster method consists in solving approximate equations, such as one of the numerous forms the Boussinesq or Serre-Green-Naghdi equations. However, these mathematical systems are unable to retain the complete dispersive and nonlinear properties of the water wave problem.

An intermediate approach consists in solving the fully nonlinear and dispersive potential flow model, reformulated as the Zakharov equations [20]. This approach resolves the potential flow problem by advancing in time free surface quantities only. Several approaches can be considered to solve the Zakharov equations, such as the Hamiltonian approach with coupled modes [11, 12], the extension of the high-order spectral (HOS) method to variable bottom cases [6], or the use of finite differences schemes [4]. In this study, a spectral approach is applied in the vertical dimension using Chebyshev polynomials, following Tian and Sato [18]. This approach is accurate and converges quickly as a function of the number of polynomials used, as demonstrated in Benoit et al. [3], Raoult et al. [13], Yates and Benoit [19].

One limitation of the Zakharov equations is the assumption of a non-overturning free surface, which precludes direct modeling of wave breaking. In order to overcome this limitation, some of the effects of wave breaking can be simulated by dissipating energy at the time and location a wave is considered to break. The activation of the dissipation, or the onset criterion of breaking, can be triggered by different types of thresholds, which are generally either geometrical, kinematic, or energetic.

In this work, two breaking criteria and two dissipation methods are implemented in a numerical code solving the Zakharov equations (code whispers3D). The simulation results are compared with experimental measurements for waves breaking over a submerged bar, confirming the applicability of the proposed modeling strategies, both for regular and irregular wave conditions.

II – Method

II – 1 Overview of the system of equations

For an inviscid and homogeneous fluid of constant density, potential flow theory can be used if the flow is assumed irrotational. In the following, the domain is restricted to two dimensions in the vertical plane (x, z) with x being the horizontal axis and z the vertical axis positive upward, with $z = 0$ at the still water surface. In this case, the velocity vector $\underline{u}(x, z, t) = (u, w)$ can be expressed as the spatial gradient of the velocity potential $\Phi(x, z, t)$, such that $\underline{u} = \nabla\Phi = (\Phi_x, \Phi_z)$. The velocity potential must then satisfy the Laplace equation in the fluid domain: $\Delta\Phi = 0$.

The Laplace equation is supplemented with boundary conditions at the free surface, bottom, and lateral boundaries. The seabed, $z = -h(x)$, is considered impermeable, fixed and smooth, such that: $\Phi_x h_x + \Phi_z = 0$. The free surface, $z = \eta(x, t)$, is continuous and non-overturning. The lateral boundary conditions can be periodic, Dirichlet or Neumann type. After assuming uniform atmospheric pressure at the free surface (by convention set to 0), and defining the velocity potential at the free surface as $\psi(x, t) = \Phi(x, z = \eta(x, t), t)$, the nonlinear free surface boundary conditions are formulated as the so-called Zakharov equations [20]:

$$\eta_t = -\eta_x\psi_x + W(1 + (\eta_x)^2), \tag{1}$$

$$\psi_t = -g\eta - \frac{1}{2}(\psi_x)^2 + \frac{1}{2}W^2(1 + (\eta_x)^2), \tag{2}$$

where $W(x,t)$ is the vertical velocity at the free surface $W(x,t) = \Phi_z(x, z = \eta(x,t), t)$, and $g = 9.81$ m/s^2 is the acceleration due to gravity.

Eqs. (1-2) involve only free surface variables, depending on x and t solely. To integrate these equations in time, a Dirichlet to Neumann (DtN) problem must be solved to determine W from (η, ψ), as described in Yates and Benoit [19], Raoult et al. [13] and Benoit et al. [3].

The DtN problem is solved by resolving a Laplace boundary value problem (BVP) for the potential Φ in the fluid domain:

$$\Phi_{xx} + \Phi_{zz} = 0 \qquad \text{in the fluid domain,} \tag{3}$$

$$\Phi(x,\eta) = \psi(x) \qquad \text{on } z = \eta(x,t), \tag{4}$$

$$h_x \Phi_x + \Phi_z = 0 \qquad \text{on } z = -h(x). \tag{5}$$

II – 2 Numerical implementation

To solve the above BVP problem (3-5) and march Eqs. (1-2) in time, a numerical code, called whispers3D, is being developped at Centrale Marseille and Irphé lab. It combines high-order finite difference schemes to approximate the horizontal derivatives with a spectral method in the vertical dimension using the Chebyshev-tau approach, following the work of Tian and Sato [18]. With this method, the potential is approximated by a linear combination of Chebyshev polynomials of the first kind, $T_n(s), n = 0, 1, ..., N_T$ for $s \in [-1, 1]$:

$$\Phi(x,z) = \varphi(x,s) \approx \sum_{n=0}^{N_T} a_n(x) T_n(s), \tag{6}$$

where s is the scaled vertical coordinate, varying from -1 at the bottom to $+1$ at the free surface:

$$s(x,z,t) = \frac{2z + h(x) - \eta(x,t)}{h(x) + \eta(x,t)}, \tag{7}$$

and N_T is the maximum order of the Chebyshev polynomial used in the approximation. In the following simulations, N_T is set to 7, which was found to be a good compromise between computational speed and accuracy [19, 13]. The resulting linear system of equations on the $a_n(x)$ coefficients is solved here using a GMRES algorithm with Incomplete L-U preconditioning. The integration in time is performed with a third-order Runge Kutta scheme SSPRK$(3,3)$. At the domain inlet, incident waves are generated by reconstructing η and ψ from a measured wave signal by decomposing it using the linear wave theory as a sum of independent sinusoidal waves. A relaxation zone in the first part of the domain allows imposing this incident wave condition progressively in space while absorbing reflected waves propagating in the direction of the inlet boundary. At the opposite end of the domain, an absorbing relaxation zone forces the solution to 0 with a progressive transition in space to dampen waves and limit wave reflections.

II – 3 Modeling breaking waves

To include a representation of wave breaking in the model presented above, three ingredients are needed: (i) a criterion triggering the onset of breaking for a wave reaching a limit of stability, (ii) a criterion to determine the termination of breaking, and (iii) a method dissipating wave energy during the breaking event. Regarding item (i), in the literature, several criteria can be found to activate breaking, which can be grouped into three families: geometric, kinematic or energetic.

In this work, two methods are tested to initiate a breaking event. The first method (denoted B1 in the following) is geometric and uses the slope of the wave front to trigger the breaking [15]. Wave breaking is initiated when the slope of the wave, $\beta(x,t)$, is greater than a threshold value: $\beta_{\max}$ (see Figure 1). In the literature, values of $\beta_{\max}$ range from 28 to 38°, depending

on the type of wave and the local bottom slope. Cienfuegos et al. [5] recommended setting $\beta_{\max}$ between 28 and 32° for spilling breakers, or between 35 and 36° for plunging breakers. Here, after a sensitivity study, a value of $\beta_{\max} = 35°$ was selected and will be used for all tests presented hereafter.
The second method (denoted B2 in the following) is based on the local energy flux velocity [1]. For two dimensional flows, this breaking criterion can be reduced to a dynamical criterion: $B_x = u_1(x_c, t)/C$, where C is the (local) crest velocity, x_c the position of the crest, and u_1 the horizontal velocity at the free surface. Wave breaking is initiated when $B_x = u_1(x_c, t)/C > B_{\max}$. According to Barthelemy et al. [1], the threshold $B_{\max}$ should be chosen in the range $[0.85, 0.86]$ for waves in deep water and intermediate depth; the same authors expect a similar threshold to be valid for shallow water conditions. Saket et al. [14] re-examined available data sets and reduced the interval for $B_{\max}$ to 0.84 ± 0.016. A threshold value of $B_{\max} = 0.84$ will be used throughout the current study.

Figure 1 presents the characteristics of a breaking wave with celerity C. h_c is the water depth under the crest located at x_c, h_t is the depth under the front trough at x_t, H is the wave height, and β is the angle of the slope of the wave front relative to the horizontal. The interval $[x_b, x_f]$ is the zone of energy dissipation, as defined by Guignard and Grilli [7].

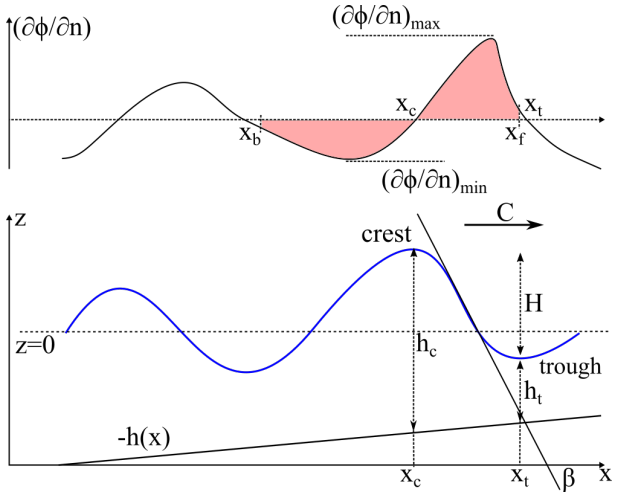

Figure 1 – Definition of geometric and kinematic parameters for a breaking wave, based on [7].

Once the onset of wave breaking is detected, a dissipation term needs to be applied on a specific region of the breaking wave. We consider and compare two methods, both relying on adding a term, P_{surf}, similar to a surface pressure, to Eq. (2):
The first method (denoted HJ in the following) uses an analogy with a hydraulic jump to estimate the pressure term P_{surf} [7]. The zone where the pressure is applied extends on both sides of the breaking crest between the abscissas x_f and x_b (see Figure 1) determined by:

$$\left| \frac{\partial \Phi}{\partial n} \Big/ \left(\frac{\partial \Phi}{\partial n} \right)_{\min,\max} \right| > \epsilon \quad \text{for} \quad x \in [x_b, x_f]\,, \tag{8}$$

with ϵ being a small threshold value (in our case: $\epsilon = 10^{-5}$). The normal derivative of the potential Φ at the free surface is given by:

$$\frac{\partial \Phi}{\partial n}(\eta) = n \cdot \nabla \Phi = \eta_t = -\eta_x \psi_x + W(1 + (\eta_x)^2), \tag{9}$$

where n is the normal vector (non unit) to the free surface.
The pressure P_{surf}, non zero in the breaker zone (x_f, x_b), is defined as:

$$P_{surf} = \nu_b S(x) \frac{\partial \Phi}{\partial n}(x), \tag{10}$$

where $S(x)$ is a function ensuring a smooth transition across areas with and without breaking. It varies sinusoidally from 0 to 1 at the borders $[x_b, x_{b1}]$ and $[x_{f1}, x_f]$ of the breaker zone, such that $x_{b1} = x_b - \alpha(x_b - x_f)$ and $x_{f1} = x_f - \alpha(x_b - x_f)$ (α is defined depending on the case, and $\alpha = 0.1$ is used here as suggested in [7]). The absorption coefficient, ν_b, is defined as:

$$\nu_b = \mu P_{jump} \left(\int_{x_b}^{x_f} S(x) \left(\frac{\partial \Phi}{\partial n}(x) \right)^2 dx \right)^{-1}, \tag{11}$$

where μ is a coefficient controlling the magnitude of the dissipation. Svendsen et al. [17] recommend selecting a value close to 1.5. In the following, $\mu = 1.0$ is used. P_{jump} is the power dissipated in a turbulent bore [10], defined by [7]:

$$P_{jump} = gC \frac{hH^3}{4h_c h_t}. \tag{12}$$

The second dissipation method uses an eddy viscosity model to dissipate energy due to breaking (denoted EVM in the following). Following the work of Kennedy et al. [8] and Kurnia and van Groesen [9], the pressure term can be obtained as a solution of the equation:

$$\partial_x P_{surf} = \frac{1}{h + \eta} \partial_x F, \quad \text{for } x \in [x_c, x_t], \tag{13}$$

where $F = \beta(h + \eta)(\partial_t \eta)^2$. Eq. (13) is derived by imposing the additional condition that the total wave momentum should be conserved for waves propagating over a flat bottom. The term $\beta = \delta^2 B(\partial_t \eta)$ with $\delta \in [1, 1.2]$ [8] determines the magnitude of dissipation, with B being a function between 0 and 1 controlling the initiation and cessation of the breaking process. In the following simulations, δ is set to 1.2. The function B is modified in the form of a coefficient varying linearly from 0 to 1 over 8 time steps. This reduces the occurrence of instabilities due to the inclusion of P_{surf} in Eq. 2, and B is also simplified since the breaking onset is determined by either the conditions B1 or B2. In order to compute P_{surf}, Eq. (13) needs to be integrated, which is done using a simple Euler method in the current implementation. Once calculated, the pressure is added to Eq. (2) only on the front face of the breaking wave, between x_c and x_t.

Regarding breaking termination (item ii), for both HJ and EVM methods, the dissipation is stopped when the slope of the wave front becomes smaller than $\beta_{\min} = 8°$ [5].

When computing the breaking onset B2 and/or the pressure term with the HJ method, an accurate estimation of phase speed C of the wave is needed. Here, following [9, 16], a partial Hilbert transform is used to determine the instantaneous wave number k and to deduce the crest speed using the linear dispersion relation:

$$C(x,t) = \sqrt{g \frac{\tanh(k(x,t)h)}{k(x,t)}}. \tag{14}$$

To compute k, the partial Hilbert transform is used with respect to x, which is defined by:

$$\mathbb{H}[\eta(x,t)] = \frac{1}{\pi} p.v. \int_{-\infty}^{+\infty} \frac{\eta(x',t)}{x - x'} dx', \tag{15}$$

where $p.v.$ is the Cauchy principal value of the integral. The Hilbert transform is used to express the phase function, which allows computing the wave number as:

$$k(x,t) = \frac{1}{\eta^2 + \mathbb{H}[\eta]^2} \left(\eta \mathbb{H}_x[\eta] - \mathbb{H}[\eta] \eta_x \right). \tag{16}$$

III – Results

III – 1 Experimental set-up and numerical settings

In order to evaluate the methods for modeling wave breaking, the numerical simulations made with the modified version of whispers3D are compared with laboratory experiments performed by Beji and Battjes [2] for regular and irregular waves. The experiments were conducted in a wave flume with a water depth of 0.40 m, equipped with a wave-board located at $x = 0$ m. The flume contains a trapezoidal bar: the water depth first decreases with a slope of $1 : 20$ from $x = 6$ m to $x = 12$ m, followed by 2 m long horizontal section with a water depth of 0.10 m. From $x = 14$ to 17 m, the depth increases with a slope of $1 : 10$. From $x = 17$ m on, the depth is again uniform at 0.40 m (see Figure 3). 8 wave gauges, located at located at $x = 6$, 11, 12, 13, 14, 15, 16 and 17 m, measure the free surface elevation.
For the numerical simulations, the signal recorded at the first probe (located at $x = 6$ m) is used to generate the incident wave conditions imposed at the inlet boundary of the numerical model. The numerical domain reproduces the experimental bathymetry with a uniform discretization, $\Delta x = 0.02$ m, with the domain extending from $x = 3$ m to $x = 20$ m. The simulations are run with a constant time-step of $\Delta t = 0.02$ s.
For both regular and irregular waves, simulations were run combining both onset criteria (B1 and B2) and both dissipation formulations (HJ and EVM). The simulations are named after the selected combination (breaking criterion+dissipation method), for example: simulation B1_HJ uses the criterion B1 to trigger the activation of the dissipation HJ. As mentioned above, the simulations results are run with $\beta_{\max} = 35°$, $B_{max} = 0.84$, $\mu = 1.0$ and $\delta = 1.2$.

III – 2 Wave breaking for regular waves over a submerged bar

We first consider one experiment conducted with incident regular waves having a wave height $H = 0.054$ m and a period $T = 2.5$ s, resulting in a breaker-type classified as plunging [2].
Figure 2 presents comparisons of measured and simulated time series of the free surface elevation at 3 different positions. The simulated time series from the four combinations are in very close agreement. In particular, the combinations using the same dissipation method produce nearly identical results, showing no significant influence of the breaking criterion in this case (B1 used $\beta_{\max} = 35°$ and B2 used with $B_{\max} = 0.84$). This allows comparing the effects of the dissipation method (HJ or EVM) and shows that both methods reproduce the wave decay similarly despite differences in their formulation and their zone of application. Comparing the time series to experimental data, the different simulation results follow closely the experimental data, although differences arises regarding secondary peaks. Nevertheless, the shape of the waves remains similar to the experimental data showing that nonlinear effects are captured well by the model.

Figure 3 shows the envelop of wave crests and troughs from the simulations and the experiments. Again, the wave envelops from the simulations are matching closely one another. The curves from B1_HJ and B2_HJ are even superimposed. The same results occurs for B1_EVM and B2_EVM, confirming the equivalence of both breaking criteria B1 with $\beta_{\max} = 35°$ and B2 with $B_{\max} = 0.84$, for this specific wave condition. Comparing with experimental data, the evolution of envelop is reproduced well by the breaking methods with a slight underestimation of the free surface elevation after $x = 14$ m.
During the simulations, wave breaking was observed to occur on average between $x = 12.1$ and 14.4 m for simulations using the HJ dissipation method, and between $x = 12.1$ and 14.1 m for simulations using the EVM dissipation method, confirming the similarity of the dissipation methods.

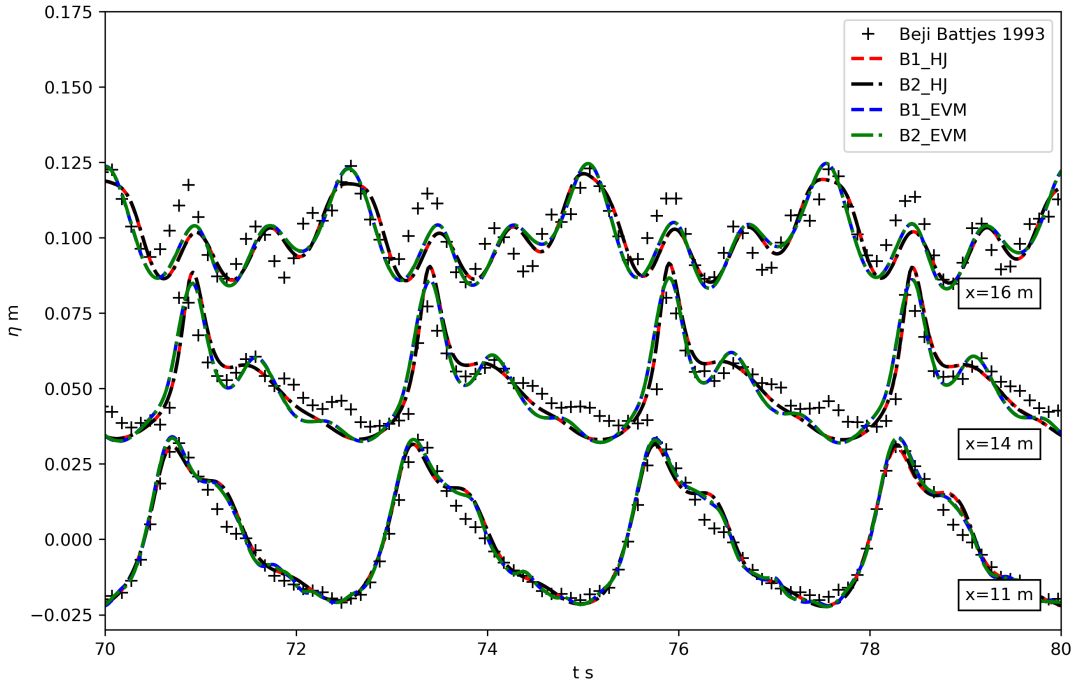

Figure 2 – Time series of the free surface elevation for a test with regular waves ($H = 0.054$ m, $T = 2.5$ s). Comparison between experimental measurements and numerical simulations with whispers3D using different combinations of breaking criterion and dissipation method. The curves at each position, x, are offset by 0.05 m for clarity.

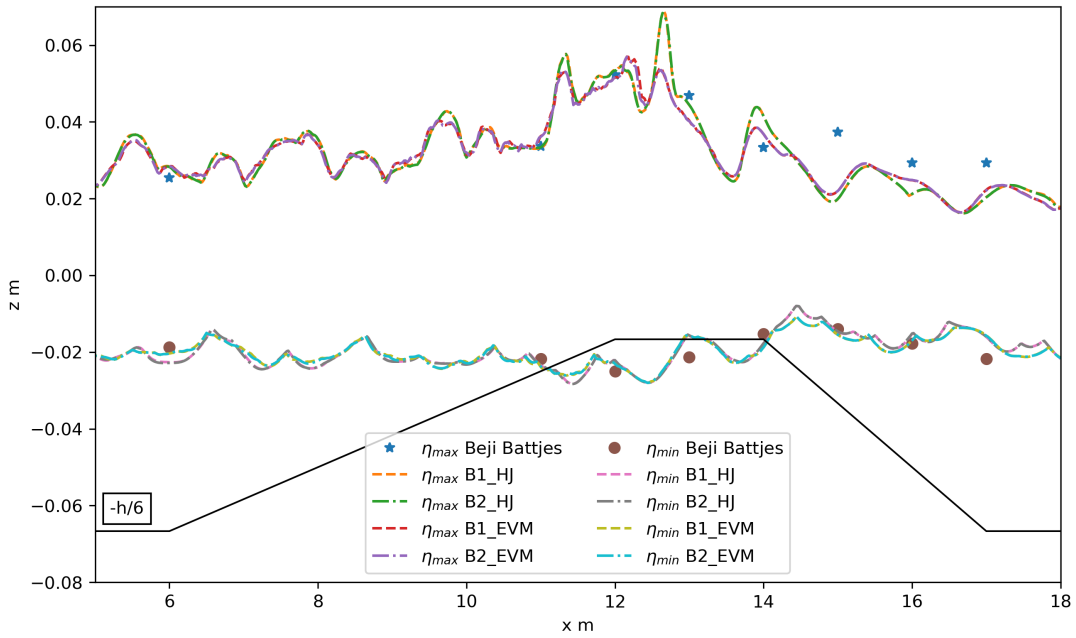

Figure 3 – Comparison of the wave envelops of the experimental data and numerical simulation results for a test with regular waves ($H = 0.054$ m, $T = 2.5$ s), using different combinations of breaking criterion and dissipation method.

III – 3 Wave breaking for irregular waves over a submerged bar

We then consider an experiment with the same bathymetry but with irregular waves characterized by a JONSWAP type spectrum having a significant wave height $H_{m_0} = 0.049$ m and a peak

period $T_p = 2.5$ s [2].
During the simulations, breaking does not occur for every wave passing over the bar. Only the largest waves break. The results indicate that, on average, breaking starts around $x = 12.4$ m and stops around $x = 14.4$ m. However, some waves start breaking before $x = 10$ m.
Figure 4 presents time series of the free surface elevation from the simulations and the experiments at 3 different positions. As for the regular wave condition, the time series issued from the simulations have little discrepancies between one another, despite the different methods used for the breaking onset and the energy dissipation. Comparing with the experimental data, good agreement is also found with the simulation results. Nonetheless, some differences appear progressively along the wave flume after the propagation of a breaking wave.

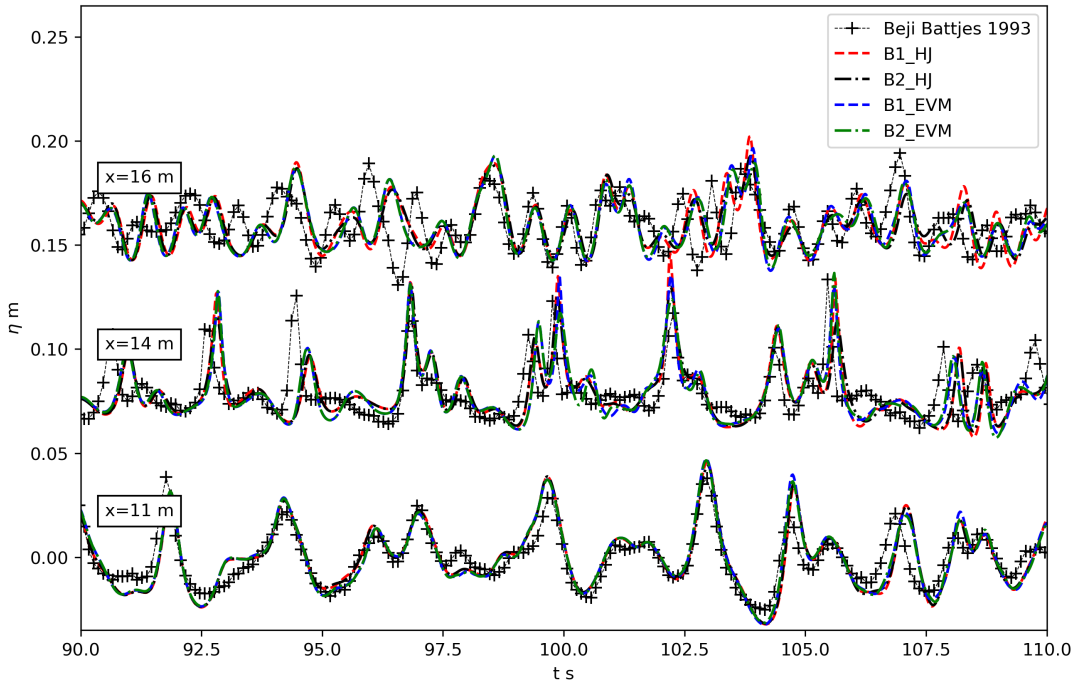

Figure 4 – Time series of the free surface elevation for a test with irregular waves ($H_{m_0} = 0.049$ m, $T_p = 2.5$ s). Comparison between experiment and numerical simulations with whispers3D using different combination of breaking criterion and dissipation method. The curves at each position, x, are offset by 0.08 m for clarity.

Figure 5 shows the envelop of wave crests and troughs from the simulations and the experiments. The envelops from the simulations agree well with each other as well as with the experimental measurements. Differences appear around $x = 11$ m, where the maximum value of the free surface is reached near $x = 10$ m in the simulations and at $x = 11$ m in the experiments. The time series at $x = 11$ m shows that this occurs for only one particular wave. Note that due to the lack of wave probes between $x = 6$ m and $x = 10$ m, it is difficult to perform a detailed analysis of the simulated wave crest envelops in this zone that shows local amplification of the largest waves prior to breaking. Nonetheless, the simulations agree well with the experimental results. Comparing the evolution along the bottom profile of the significant wave height, wave asymmetry, and wave skewness along the wave flume (not shown here), it was observed that simulation results are in fair agreement with the experimental data, with a slightly better match for the simulation B2_HJ.

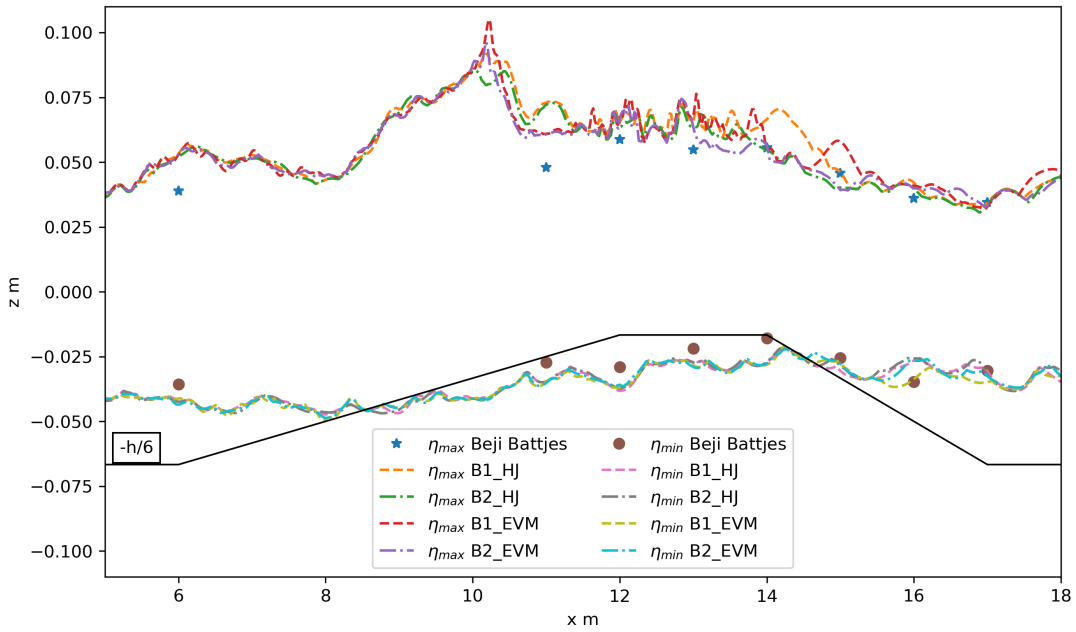

Figure 5 – Comparison of the wave envelops of the experimental data and numerical simulation results for a test with irregular waves ($H_{m_0} = 0.049$ m, $T_p = 2.5$ s), using different combinations of breaking criterion and dissipation method.

IV – Conclusions

The development and validation of wave breaking is ongoing, but preliminary numerical results indicate that the potential flow solver whispers3D, with the selected breaking onset criteria and dissipation methods is able to reproduce correctly the behavior of wave breaking in shallow water, both for regular and irregular wave conditions. The simulation results presented here are limited to wave breaking over a submerged bar, nevertheless the results and comparisons with experimental data are encouraging.

Regarding the breaking onset criterion, both the B1 and B2 methods give similar results for the simulated wave conditions. Method B2, based on the local energy flux velocity proves to be robust for shallow water conditions despite the fact the threshold $B_{\max} = 0.84$ was initially proposed and validated for waves in deep water or intermediate water depths [14]. One drawback of B2 is the need to estimate the wave velocity C, which increases the CPU resources.

Considering the dissipation formula, both methods HJ and EVM produce similar results for the tested conditions. In both methods, the position of the crest and trough of each breaking wave needs to be determined and followed in time. Using the hydraulic jump (HJ) method generally produce more stable simulations but requires the estimation of the wave celerity. The eddy viscosity method (EVM) only requires calibrating the parameter δ, but needs the integration of Eq. (13). Furthermore, at least in its current implementation, this method sometimes produced unstable simulations.

Future work will address additional validation of the code with other experimental data sets, development of the code to model run-up events on slopes, and the extension of the model to three-dimensional cases to simulate more realistic wave conditions.

Acknowledgements

This work was carried out in the framework of the DEPHYMAN project, funded by the Labex MEC (Mécanique et Complexité) with reference ANR-10-LABX-0092 and the A*MIDEX project (ANR-11-IDEX-0001-02), funded by the Investissements d'Avenir French Government program

managed by the French National Research Agency (ANR).

C. Papoutsellis, M. Benoit and M. Yates also acknowledge support from the DiMe project, which benefits from French Government support managed by the ANR under the program Investissements d'Avenir with the reference ANR-10-IEED-0006-14.

References

[1] X. Barthelemy, M. L. Banner, W. L. Peirson, F. Fedele, M. Allis, and F. Dias. On a unified breaking onset threshold for gravity waves in deep and intermediate depth water. *Journal of Fluid Mechanics*, 841:463–488, 2018.

[2] S. Beji and J. Battjes. Experimental investigation of wave propagation over a bar. *Coastal Engineering*, 19(1):151–162, 1993.

[3] M. Benoit, C. Raoult, and M. L. Yates. Analysis of the linear version of a highly dispersive potential water wave model using a spectral approach in the vertical. *Wave Motion*, 74: 159–181, 2017.

[4] H. B. Bingham and H. Zhang. On the accuracy of finite-difference solutions for nonlinear water waves. *Journal of Engineering Mathematics*, 58(1):211–228, 2007.

[5] R. Cienfuegos, E. Barthélemy, and P. Bonneton. Wave-breaking model for Boussinesq-type equations including roller effects in the mass conservation equation. *Journal of Waterway, Port, Coastal, and Ocean Engineering*, 136(1):10–26, 2010.

[6] M. Gouin, G. Ducrozet, and P. Ferrant. Development and validation of a non-linear spectral model for water waves over variable depth. *European Journal of Mechanics - B/Fluids*, 57: 115–128, 2016.

[7] S. Guignard and S. T. Grilli. Modeling of wave shoaling in a 2D-NWT using a spilling breaker model. In *ISOPE-I-01-253*, ISOPE, 2001. International Society of Offshore and Polar Engineers.

[8] A. B. Kennedy, Q. Chen, J. T. Kirby, and R. A. Dalrymple. Boussinesq modeling of wave transformation, breaking, and runup. I: 1D. *Journal of Waterway, Port, Coastal, and Ocean Engineering*, 126(1):39–47, 2000.

[9] R. Kurnia and E. van Groesen. High order Hamiltonian water wave models with wave-breaking mechanism. *Coastal Engineering*, 93:55–70, 2014.

[10] H. Lamb. *Hydrodynamics*. Univ. Press, Cambridge, 6th ed., repr., transf. to digital printing edition, 1993.

[11] C. Papoutsellis, A. Charalampopoulos, and G. Athanassoulis. Implementation of a fully nonlinear Hamiltonian Coupled-Mode Theory, and application to solitary wave problems over bathymetry. *European Journal of Mechanics - B/Fluids*, 72:199–224, 2018.

[12] C. E. Papoutsellis, M. L. Yates, B. Simon, and M. Benoit. Fully nonlinear modeling of nearshore wave propagation including the effects of wave breaking. International Conference on Coastal Engineering, Baltimore (USA), 2018.

[13] C. Raoult, M. Benoit, and M. L. Yates. Validation of a fully nonlinear and dispersive wave model with laboratory non-breaking experiments. *Coastal Engineering*, 114:194–207, 2016.

[14] A. Saket, W. L. Peirson, M. L. Banner, X. Barthelemy, and M. J. Allis. On the threshold for wave breaking of two-dimensional deep water wave groups in the absence and presence of wind. *Journal of Fluid Mechanics*, 811:642–658, 2017.

[15] H. A. Schäffer, P. A. Madsen, and R. Deigaard. A Boussinesq model for waves breaking in shallow water. *Coastal Engineering*, 20(3):185–202, 1993.

[16] P. Stansell and C. MacFarlane. Experimental investigation of wave breaking criteria based on wave phase speeds. *Journal of Physical Oceanography*, 32(5):1269–1283, 2002.

[17] I. A. Svendsen, P. A. Madsen, and J. B. Hansen. Wave characteristics in the surf zone. In *International Conference on Coastal Engineering 1978*, pages 520–539, Hamburg, Germany, 1978. American Society of Civil Engineers.

[18] Y. Tian and S. Sato. A numerical model on the interaction between nearshore nonlinear waves and strong currents. *Coastal Engineering Journal*, 50(4):369–395, 2008.

[19] M. L. Yates and M. Benoit. Accuracy and efficiency of two numerical methods of solving the potential flow problem for highly nonlinear and dispersive water waves. *International Journal for Numerical Methods in Fluids*, 77(10):616–640, 2015.

[20] V. E. Zakharov. Stability of periodic waves of finite amplitude on the surface of a deep fluid. *Journal of Applied Mechanics and Technical Physics*, 9(2):190–194, 1968.